Epitaxial Growth of CoGa on GaAs by Organometallic Chemical Vapor Deposition

Francis Maury,† A. Alec Talin, Herbert D. Kaesz,* and R. Stanley Williams

Department of Chemistry and Biochemistry, University of California, Los Angeles, California 90024-1569

Received July 24, 1992. Revised Manuscript Received November 9, 1992

Epitaxial layers of CoGa have been grown successfully for the first time on (100)GaAs by organometallic chemical vapor deposition, using $(\eta^5\text{-}C_5H_5)Co(CO)_2$ and Et_3Ga as precursors. The composition of the intermetallic films is adjustable by control of the composition of the gas phase in such a way that no detectable lattice mismatch is observed between Ga-rich CoGa films and the GaAs substrate. However, the films deposited with an excess of Co exhibit a metastable α (fcc) structure corresponding to a $Co_{1-x}Ga_x$ solid solution. These films are structurally incompatible with GaAs, and were also found to react with GaAs above 400 °C to form CoAs. From gas phase compositions $Et_3Ga/CoCp(CO)_2 \geq 5$, the CoGa films have the cubic β (CsCl) structure and grow epitaxially on (100)GaAs in the temperature range 260–300 °C. The growth rate of these films has been investigated as a function of the deposition parameters. The Ga-rich β-CoGa films are thermodynamically stable on GaAs at 500 °C, which is the temperature used for GaAs epitaxial growth by this technique. This suggests that CoGa is a good candidate material for the fabrication of buried metal/GaAs heterostructures by organometallic vapor-phase epitaxy.

Introduction

Contact metallization is currently a limiting factor in III–V semiconductor device technology. This is because most single element metals are thermodynamically unstable with respect to III–V semiconductor such as GaAs. Chemical reactions at metal/semiconductor interfaces lead to changes in the electrical properties of the contact. To avoid this instability, the metallic film should be thermodynamically stable toward the semiconductor compound. From this point of view, the metal–III–V ternary phase diagrams provide a useful framework for the selection of the metallization materials.[1]

Furthermore, if a single-crystalline metallic film is grown epitaxially on the semiconductor, the stability of the interface will be improved, and it will possible to grow an additional semiconductor epilayer on top. Metals which are both thermodynamically stable and lattice matched to the semiconductor will allow the preparation of new and useful electronic devices based on buried metal/semiconductor heterostructures, as was recently demonstrated for metal alumide/semiconductor systems.[2-5]

Transition metal gallides and aluminides have attracted a growing interest because they are both thermodynamically stable[6-8] and have a cubic structure (CsCl, B2 type) with a lattice constant close to half the lattice constant of GaAs.[9] Epitaxial growth of these intermetallic phases was successfully achieved by physical deposition techniques such as evaporation followed by annealing, e.g., CoGa/GaAs,[10] NiAl/GaAs,[11] and PtAl/GaAs[12] or directly by molecular beam epitaxy (MBE), e.g., CoAl,[2,13] NiAl,[3-5] CoGa,[14-19] NiGa,[20] RhGa,[21] PtGa,[22] and $AuGa_2$.[23] The suitability of rare-earth arsenides for epitaxial metallization was also investigated by MBE, e.g., ErAs,[24,25] LuAs,[25] and YbAs,[26] as well as metal arsenide, Rh_2As.[27]

However, the organometallic vapor-phase epitaxy technique (OMVPE), which is conventionally used for the deposition of the III–V layers, has several attractive advantages over physical deposition techniques such as its versatility and suitability for large-scale production

† Permanent address: CNRS-URA 445, Ecole Nationale Supérieure de Chimie, 118 route de Narbonne, 31077 Toulouse cedex, France

(1) Tsai, C. T.; Williams, R. S. *J. Mater. Res.* **1986**, *1*, 352.
(2) Tanaka, M.; Ikarashi, N.; Sakakibara, H.; Ishida, K.; Nishinaga, T. *Appl. Phys. Lett.* **1992**, *60*, 835.
(3) Sands, T.; Harbison, J. P.; Chan, W. K.; Schwarz, S. A.; Chang, C. C.; Palmstrøm, C. J.; Keramidas, V. G. *Appl. Phys. Lett.* **1988**, *52*, 1216.
(4) Harbison, J. P.; Sand, T.; Tabatabaie, N.; Chan, W. K.; Flores, L. T.; Keramidas, V. G. *Appl. Phys. Lett.* **1988**, *53*, 1717.
(5) Sands, T.; Harbison, J. P.; Tabatabaie, N.; Chan, W. K.; Gilchrist, H. L.; Schwarz, S. A.; Schwartz, C. L.; Florez, L. T.; Keramidas, V. G. *Mater. Res. Soc. Symp. Proc.* **1989**, *144*, 571.
(6) Beyers, R.; Kim, K. B.; Sinclair, R. *J. Appl. Phys.* **1987**, *61*, 2195.
(7) Kaesz, H. D.; Williams, R. S.; Hicks, R. F.; Zink, J. I.; Chen, Y.-J.; Müller, H.-J.; Xue, Z.; Shuh, D. K.; Kim, Y.-K. *New J. Chem.* **1990**, *14*, 527.
(8) Schmid-Fetzer, R. *J. Electron. Mater.* **1988**, *17*, 193.
(9) Villars, P.; Calvert, L. D. *Pearson's Handbook of Crystallographic Data for Intermetallic Phases*; American Society for Metals: Metals Park, OH, 1985; Vols. 2 and 3.
(10) Shiau, F. Y.; Chang, Y. A.; Chen, L. J. *J. Electron. Mater.* **1988**, *17*, 433.
(11) Sands, T. *Appl. Phys. Lett.* **1988**, *52*, 197.
(12) Ko, D.-H.; Sinclair, R. *Mater. Res. Soc. Symp. Proc.* **1990**, *181*, 333.
(13) Tanaka, M.; Sakakibara, H.; Nishinaga, T. *Appl. Phys. Lett.* **1991**, *59*, 3115.
(14) Baugh, D. A.; Talin, A. A.; Williams, R. S.; Kuo, T.-C.; Wang, K. L. *J. Vac. Sci. Technol. B* **1991**, *9*, 2154.
(15) Kim, Y. K. Dissertation Thesis; University of California Los Angeles, 1990.
(16) Palmstrøm, C. J.; Fimland, B.-O.; Sands, T.; Garrison, K. C.; Bartynski, R. A. *J. Appl. Phys.* **1989**, *65*, 4753.
(17) Garrison, K. C.; Palmstrøm, C. J.; Bartynski, R. A. *Mater. Res. Soc. Symp. Proc.* **1989**, *144*, 613.
(18) Palmstrøm, C. J.; Garrison, K. C.; Fimland, B.-O.; Sands, T.; Bartynski, R. A. *Mater. Res. Soc. Symp. Proc.* **1989**, *144*, 583.
(19) Zhu, J. G.; Carter, C. B.; Palmstrøm, C. J.; Garrison, K. C. *Appl. Phys. Lett.* **1989**, *55*, 39.
(20) Guivarc'h, A.; Guerin, R.; Secoue, M. *Electron. Lett.* **1987**, *23*, 1004.
(21) Guivarc'h, A.; Secoue, M.; Guenais, B. *Appl. Phys. Lett.* **1988**, *52*, 948.
(22) Sadwick, L. P.; Wang, K. L.; Shuh, D. K.; Kim, Y. K.; Williams, S. T. *Mater. Res. Soc. Symp. Proc.* **1989**, *144*, 595.
(23) Lince, J. R.; Williams, S. T. *J. Vac. Sci. Technol. B* **1985**, *3*, 1217.

0897-4756/93/2805-0084$04.00/0

applications.[28] Previously, we have reported on the polycrystalline deposition of one of such thermodynamically stable metal in a hot-wall chemical vapor deposition (CVD) reactor, namely, the compound CoGa from the single-source precursor $(OC)_4CoGaCl_2(THF)$ (THF = tetrahydrofuran, C_4H_8O). The film deposited at 500 °C was found to retain the stoichiometry Co:Ga = 1:1 fixed by the precursor.[29] However, this intermetallic phase exists over a wide range of composition[30] and both the best lattice match and the highest thermodynamic stability occur for Ga-rich compositions of 61 at. % Ga[14] and 55 at. % Ga,[31] respectively.

In this paper, we report on the successful epitaxial growth of CoGa films on (100)GaAs using the separate sources $CoCp(CO)_2$ ($Cp = \eta^5$-C_5H_5) and Et_3Ga ($Et = C_2H_5$), in a cold-wall laminar flow CVD reactor. The influence of the deposition parameters on the composition, the structure, and the growth rate of the films is discussed. These results were recently reported in abbreviated form.[32]

Experimental Section

Precursor Selection. Different organometallic Co compounds have been previously used as precursors in CVD. However, liquid precursors are more desirable than solid compounds in view of the stability and the controlability of the gas-phase composition, which is an important requirement for the growth of a binary compound. The compound $CoCp(CO)_2$ was selected because it is a volatile liquid. The values of its vapor pressure, measured by the transport method near room temperature, combined with literature data at higher temperature (310–413 K),[33-35] fit the equation

$$\log p(\text{kPa}) = 9.11 - 2971.8/T\,(\text{K})$$

To have a temperature range of decomposition for the Ga precursor compatible with that of $CoCp(CO)_2$, the compound $(C_2H_5)_3Ga$ was preferred to the conventional $(CH_3)_3Ga$ source because it is known to be thermally less stable, especially under hydrogen atmosphere.[36] Its vapor pressure was temperature controlled according to literature data.[37] Both organometallic precursors were purchased from Strem Chemical, Inc.; they were used without further purification and handled following the usual precautions for air-sensitive compounds.

Apparatus and Deposition Procedure. A setup of the experimental OMCVD apparatus is shown in Figure 1. The gas lines are equipped with a purification system: gases were successively passed through a liquid nitrogen trap, an oxygen-absorbent catalyst (oxy-sorb 20–60 mesh), molecular sieves (4 Å), and filters (1 μm). Each organometallic precursor was contained in a thermostated Pyrex glass bubbler, previously filled in a glovebox. Purified helium was used as carrier gas for $CoCp(CO)_2$ to prevent premature decomposition in the bubbler, whereas purified H_2 was used for both the transport of Et_3Ga and dilution of the gas streams at the entrance of the reactor. The reactor was a horizontal air cooled quartz tube. Its overall length was 300 mm, and the inner diameter was 35 mm. The deposition temperature was monitored with a thermocouple imbedded in the heart of a stainless steel block ($50 \times 30 \times 3$ mm^3) on which the substrates were placed. A quartz ramp was positioned in front of the susceptor to keep the gas flow as smooth as possible. The susceptor was heated with an external focussed infrared lamp (1 kW) which could give substrate temperatures higher than 1000 K. The top wall of the reactor was air cooled with a fan in order to maintain a temperature of ~40 °C when the substrate temperature was maintained at 300 °C. Using the typical deposition parameters reported in Table I, a stable laminar flow (Reynolds number ≤1) was obtained in this epitaxial reactor with no evidence for convective instability zones over the susceptor. A liquid nitrogen trap was placed at the outlet of the reactor in order both to protect the vacuum system and to sample gaseous byproducts of the reaction for further analyses.

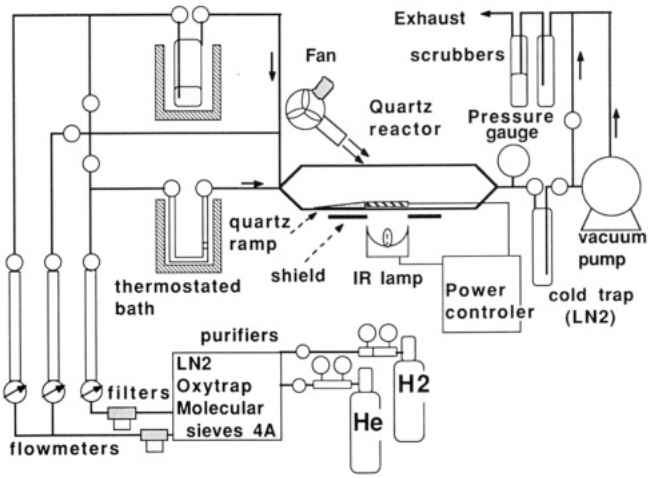

Figure 1. Setup of the OMCVD apparatus.

Table I. Typical OMCVD Conditions Used for the Epitaxial Growth of CoGa on (100)GaAs

deposition temp (°C)	260–300
total pressure (kPa)	101
total flow rate (sccm)	500
carrier gas	$He + H_2$
thermostated bath temperature (°C)	
Et_3Ga	−7 to 48 ± 0.5
$CoCp(CO)_2$	+7 to 28 ± 0.5
mole fraction	
Et_3Ga	2.05×10^{-4}–8.74×10^{-3}
$CoCp(CO)_2$	1.0×10^{-4}–6.76×10^{-4}
H_2	6.88×10^{-1}
$Et_3Ga/CoCp(CO)_2$ ratio	0.3–30.9

The (100)GaAs substrates were first degassed sequentially in hot trichloroethylene and acetone. They were then etched for 2 min in a solution composed of H_2SO_4:H_2O_2:H_2O (5:1:1 by volume) to remove surface damage, etched in a milder polishing solution of 0.5% bromine in methanol, followed by rinsing in methanol and doubly distilled water. Finally they were dried under a N_2 stream. Polycrystalline Al_2O_3 and (100)Si wafers were also used; both were first degreased as above. The Si substrates were also etched for 1 min in 49% HF solution.

The substrates were placed into the reactor immediately after cleaning and subjected to several cycles of vacuum (10^{-4} kPa) followed by H_2 pressurization. They were then heated for a few minutes at 300 °C under an H_2 stream, and the desired parameters of flow and temperatures of source and substrate were adjusted. When all the parameters were stabilized, the flow of Et_3Ga was introduced a few seconds before $CoCp(CO)_2$ in order to have a Ga terminated surface prior the growth of CoGa. At the end of the run, the substrate temperature was decreased slowly with a

(24) Palmstrøm, C. J.; Tabatabaie, N.; Allen, S. J. Jr. *Appl. Phys. Lett.* **1988**, *53*, 2608.
(25) Palmstrøm, C. J.; Garrison, K. C.; Mounier, S.; Sands, T.; Schwartz, C. L.; Tabatabaie, N.; Allen, S. J., Jr.; Gilchrist, H. L.; Miceli, P. F. *J. Vac. Sci. Technol. B* **1989**, *7*, 747.
(26) Richter, H. J.; Smith, R. S.; Herres, N.; Seelmann-Eggebert, M.; Wennekers, P. *Appl. Phys. Lett.* **1988**, *53*, 99.
(27) Guivarc'h, A.; Secoue, M.; Guenais, B.; Ballini, Y.; Badoz, P. A.; Rosencher, E. *J. Appl. Phys.* **1988**, *64*, 683.
(28) Dapkus, P. D. *J. Cryst. Growth* **1984**, *68*, 345.
(29) Chen, Y.-J.; Kaesz, H. D.; Kim, Y.-K.; Müller, H.-J.; Williams, R. S.; Xue, Z. *Appl. Phys. Lett.* **1989**, *55*, 2760.
(30) Feschotte, P.; Eggimann, P. *J. Less-Common Met.* **1979**, *63*, 15.
(31) Henig, E.-T.; Lukas, H. L.; Petzow, G. *Z. Metallkde.* **1982**, *73*, 87.
(32) Maury, F.; Talin, A. A.; Kaesz, H. D.; Williams, R. S. *Appl. Phys. Lett.* **1992**, *61*, 1075.
(33) Piper, T. S.; Cotton, F. A.; Wilkinson, G. *J. Inorg. Nucl. Chem.* **1954**, *1*, 165.
(34) King, R. B.; Stone, F. G. A. *Inorg. Chem.* **1963**, *7*, 99.
(35) Kemmitt, R. D. W.; Russel, D. R. *Comprehensive Organometallic Chemistry*; Wilkinson, G., Ed.; Pergamon Press: New York, 1982; Vol. 5, p 249.
(36) Yoshida, M.; Watanabe, H.; Uesugi, F. *J. Electrochem. Soc.* **1985**, *132*, 677.
(37) Kayser, O.; Heinecke, H., Brauers, A.; Lüth, H.; Balk, P. *Chemtronics* **1988**, *3*, 90.

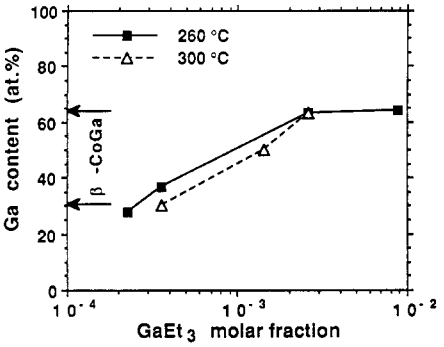

Figure 2. Variation of the film composition as a function of the Et_3Ga mole fraction in the gas stream. All the deposition parameters were kept constant including the mole fraction of $CoCp(CO)_2$, which was fixed at 2.83×10^{-4}. Data are reported for the deposition temperatures 260 and 300 °C on (100)Si. The arrows indicate the composition range of the β-CoGa phase from the phase diagram.

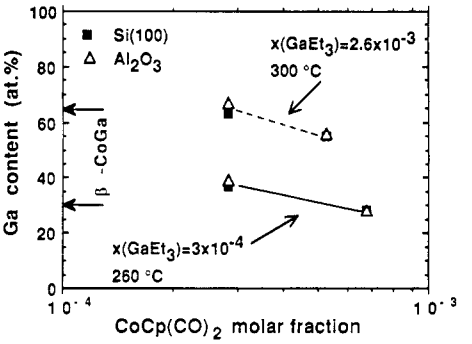

Figure 3. Variation of the film composition as a function of $CoCp(CO)_2$ mole fraction in the gas phase. Data are reported for the CoGa films deposited on (100)Si and alumina rather than GaAs to avoid interference in the EDX analysis by emissions from the substrate. The Et_3Ga mole fractions and deposition temperatures were 2.6×10^{-3} at 300 °C and 3×10^{-4} at 260 °C. The arrows indicate the composition range of the β-CoGa phase from the phase diagram.

cooling rate of 2–3 °C/min to avoid a peeling off of the film due to thermal strains.

General Instrumentation. The morphology and the thickness of the films were analyzed by scanning electron microscopy (SEM) using a Cambridge stereoscan 250 microscope. The X-ray diffraction (XRD) patterns of the samples were collected with a Phillips X-ray powder diffractometer interfaced with a microcomputer; data were typically collected in the range $2\theta = 10$–100° at 0.1° intervals with a counting time of 4–10 s at each angle. For the films on (100)Si and Al_2O_3, the composition was determined by energy-dispersive X-ray analysis (EDX; Tracor analyzer) using a $Co_{0.5}Ga_{0.5}$ bulk sample as a standard. For films on GaAs, X-ray photoelectron spectroscopy (XPS) and Auger electron spectroscopy (AES) analyses were performed using a Kratos XSAM 800 spectrometer equipped with a hemispherical electron energy analyzer. The XPS measurements were carried out using nonmonochromatized Al Kα radiation ($h\nu = 1486.6$ eV) under a base pressure of $\sim 6 \times 10^{-11}$ kPa; the XPS spectra were quantified using Scofield's coefficients.[38] The Co/Ga atomic ratio in the bulk of the films on (100)Si and Al_2O_3 (determined by EDX) agreed within 7% of that on GaAs (determined by XPS).

Results

The CoGa films were deposited under atmospheric pressure in the temperature range 260–300 °C using a gas-phase composition $Et_3Ga/CoCp(CO)_2$ in the range 0.3–30.9 (Table I). Below this temperature range no growth of CoGa films is observed because the decomposition of Et_3Ga is too low compared to that of $CoCp(CO)_2$. SEM observation of as-deposited films on (100)GaAs reveal a smooth mirrorlike and uniform surface with no evidence for grain boundaries. When the deposition temperature was increased above 300 °C, the films became silvery black on every substrate with a fine-grained surface morphology; this is evidence of high carbon contamination, resulting probably from gas-phase nucleation.

As shown in Figure 2, the Ga content of the film increases with the mole fraction of Et_3Ga up to 64 at. %, which is the upper limit of the β-CoGa phase as dictated by the phase diagram.[30] All deposition conditions were kept constant at two different temperatures, 260 and 300 °C, and the film composition was found to be only weakly dependent on the deposition temperature. Under such conditions, an increase of the Et_3Ga mole fraction beyond 2.6×10^{-3} did not increase the Ga content of the film.

Alternatively, the Ga content of the film can be decreased by increasing the mole fraction of $CoCp(CO)_2$, keeping constant the mole fraction of Et_3Ga, as shown in Figure 3. Thus, the film composition can be directly controlled from the mole ratio $Et_3Ga/CoCp(CO)_2$. The deposition of CoGa film with the stoichiometry 1:1 requires an excess of Et_3Ga in the gas phase, typically $Et_3Ga/CoCp(CO)_2 \sim 5$, because of its higher thermal stability. Similarly, a gas-phase ratio $H_3As/Et_3Ga > 10$ is required for an epitaxial growth of GaAs by this process because of the higher thermal stability of the arsenic hydride.

XPS spectra of the as-deposited samples exhibited high C 1s and O 1s peaks because of contamination of the samples during transfer through laboratory air. However, their intensity decreased sharply as a function of the time under Ar^+ sputtering; after only a few minutes, the C 1s core level was near the detection limit and all the XPS and AES peaks of Co and Ga appeared clearly. In spite of an overlap between Ga LMM Auger and the O 1s lines, there is evidence for a few atomic percent of O (<10%) even after 20 min of Ar^+ sputtering, since no further change was observed for the O 1s/Co 3p intensity ratio. As shown in Figure 4, the level of contamination of Co-rich films was slightly higher than that of Ga-rich films; after Ar^+ sputtering in the same conditions, traces of carbon were found in the former whereas no C incorporation and a lower O 1s peak were observed in Ga-rich CoGa films. This oxygen contamination was confirmed by AES analyses.

Structural Characterization. The Co-rich films containing up to 37 at. % Ga exhibit the α (fcc) structure of Co metal. This was observed on all the substrates and is clearly shown in Figure 5. The XRD patterns of two samples deposited on amorphous silica and containing 28 and 37 at. % Ga were single phased and exhibited all the diffraction peaks of α-Co metal with a dominant (111) reflection, in agreement with the JCPDS data files.[39] This result is surprising since, according to the phase diagram, films with these compositions should have either the β (CsCl) structure (stable for the composition range 29–63 at. % Ga[30]) or a biphase $\alpha + \beta$ structure. This solubility of Ga in Co metal is far beyond the limit of 21 at. % reported for the solid solution α-$Co_{1-x}Ga_x$.[30,40] The lattice constant

(38) Scofield, J. H. *J. Electron. Spectrosc. Relat. Phenom.* **1976**, *8*, 129.

(39) Joint Committee on Powder diffraction Standards, file no. 15-806.

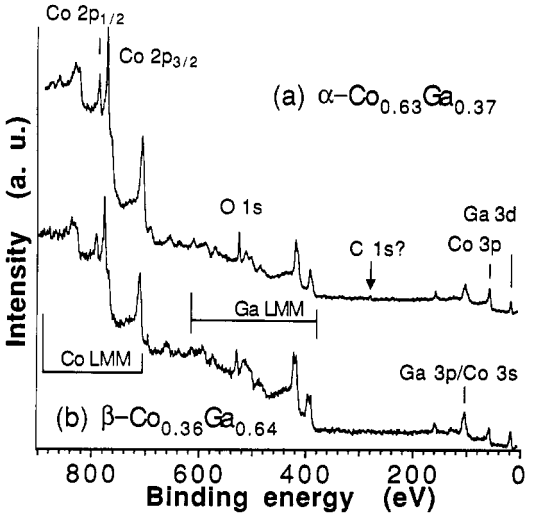

Figure 4. XPS spectra of CoGa thin films deposited by OMCVD on (100)GaAs at 300 °C: (a) α-phase containing 37 at % Ga; (b) β-phase containing 64 at. % Ga. Both spectra were recorded after Ar^+ sputtering (3 keV) under the same conditions to remove the contaminated surface layer.

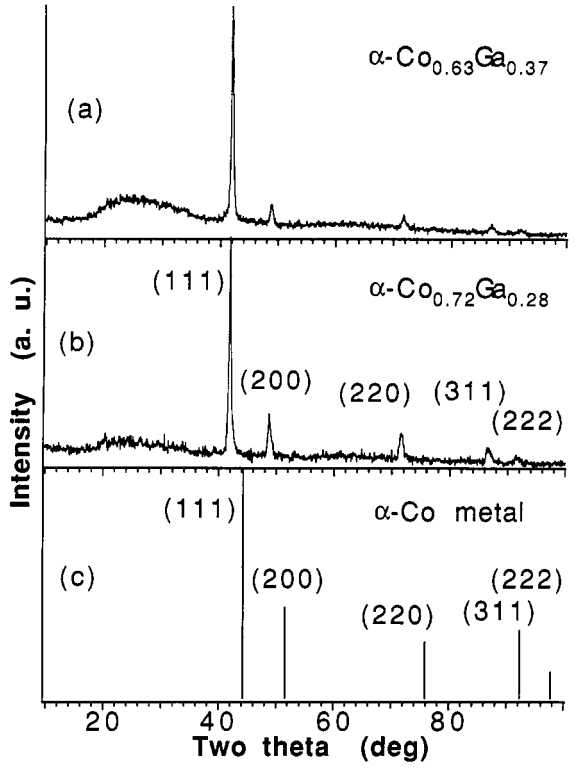

Figure 5. XRD patterns of Co-rich CoGa films deposited on amorphous silica revealing an α structure; (a) 37 at % Ga; (b) 28 at % Ga; (c) JCPDS data for α-Co metal.[39]

of this cubic phase was determined to be a = 0.372 and 0.369 nm for films containing 28 and 37 at. % Ga, respectively (Figure 5a,b). Taking into account the experimental errors and the strains in the films, these values are not significantly different ($\Delta a/a$ = 0.8%). Furthermore, they are in agreement with a value extrapolated from the literature data[40] despite the fact that the composition surpasses the limit of 21 at. % reported in that work. However, the smaller lattice parameter of α-$Co_{0.63}Ga_{0.37}$ compared to α-$Co_{0.72}Ga_{0.28}$ suggests that the

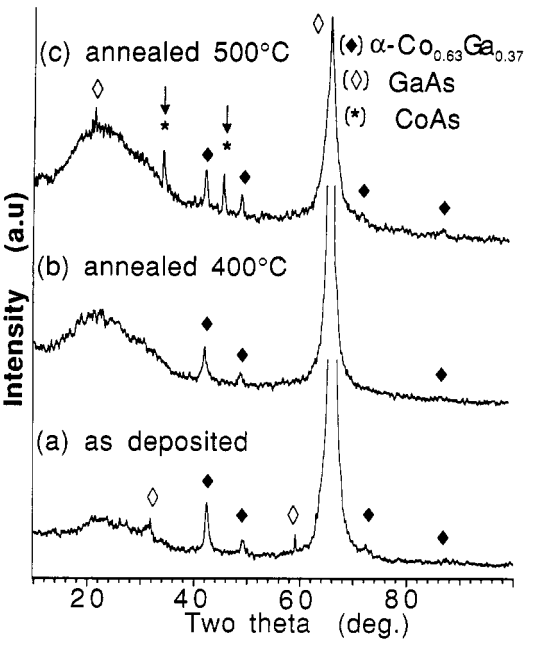

Figure 6. XRD patterns of α-$Co_{0.63}Ga_{0.37}$ thin films deposited by OMCVD at 300 °C on (100)GaAs: (a) as-deposited; (b) after annealing 1 h at 400 °C; (c) after annealing 1 h at 500 °C. Evidence of the reaction with GaAs is given by the formation of CoAs phase in c.

material could be inhomogeneous with a small volume fraction of a Ga-rich phase which is not detected by XRD. On the other hand, no evidence for a preferential orientation was found on (100)GaAs, probably because the lattice mismatch of 31% is too large.

Annealing the samples for 1 h under a N_2 gas stream reveals that these Co-rich phases are not thermodynamically stable with a GaAs substrate at 500 °C. The excess Co in these films reacts with As from the substrate for form CoAs, presumably at the interface, in agreement with the results obtained for elemental Co films on GaAs[41] (Figure 6).

As shown in Figure 7a, upon increasing the Ga content of the films near or above the stoichiometric ratio, the cubic β-CoGa phase (B2 type structure) is obtained. These CoGa films are single phased and polycrystalline on amorphous silica with a dominant (110) reflection in agreement with the powder XRD pattern of a bulk CoGa sample.

An epitaxial growth of the Ga-rich films is observed when they are deposited on (100)GaAs. The XRD pattern of an as-deposited $Co_{0.36}Ga_{0.64}$ film is shown in Figure 7b. This clearly reveals overlap between the (100) and (200) CoGa peaks and the (200) and (400) GaAs peaks. Comparison of the patterns parts a and b of Figure 7, obtained for samples with nearly the same composition (63 and 64 at. % Ga, respectively), confirms this. These films are found to be epitaxial, with no evidence for grain boundaries, but we cannot conclude from these data that they are monocrystalline. The small (110)CoGa peak observed in Figure 7b indicates that only a small volume fraction of the film is oriented with the (110) plane parallel to the substrate because the structure factor for the (110)CoGa reflection is very high compared to that for (100)CoGa (about a factor of 120). This is also true for the weak (212)$CoGa_3$ reflection, which has the highest structure

(40) Luo, H.-L.; Duwez, P. *Can. J. Phys.* **1963**, *41*, 758.

(41) Genut, M.; Eizenberg, M. *J. Appl. Phys.* **1989**, *66*, 5456.

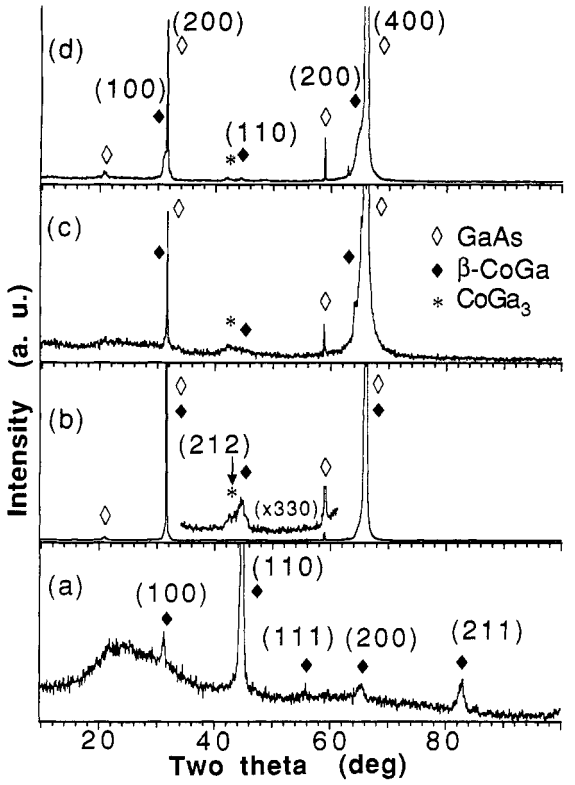

Figure 7. XRD patterns of β-CoGa thin films as-deposited: (a) 63 at. % Ga on amorphous silica; (b) 64 at. % Ga on (100)GaAs; (c) 55 at. % Ga on (100)GaAs; (d) after annealing of (c) for 1 h at 500 °C.

factor of the overall reflections of this phase[42] and gives evidence for a low level of contamination by this $CoGa_3$ phase. The presence of the $CoGa_3$ phase is explained by the phase diagram, since with 64 at. % Ga the CoGa film has a composition at the boundary between the β-CoGa single phase area and the β-CoGa + $CoGa_3$ biphased area.[30]

The lattice constant of the intermetallic compound is a function of its composition and, as shown in Figure 7c, decreasing the Ga content to 55 at. %, the (100) and (200)-CoGa XRD peaks shift to lower values of 2θ because of an increase of the CoGa lattice constant.[14,42] These reflections begin to separate from the (200) and (400)GaAs reflections, because the ca. 2% lattice mismatch.

By contrast with the Co-rich films discussed above, annealing the β-CoGa single-phase films for 1 h at 500 °C under N_2 atmosphere does not reveal any solid-state reaction at the CoGa/GaAs interface. This confirms that Ga-rich CoGa films are inert toward GaAs.[14] The composition 55 at. % Ga is that at which bulk CoGa has a minimum in its heat of formation.[31] The crystalline quality of the $Co_{0.45}Ga_{0.55}$ film improves upon annealing since the CoGa XRD peaks have slightly sharpened (Figure 7d).

Kinetics Data. The deposition rate has been determined from thickness measurements of the films on cleaved GaAs and Si samples. The growth rate of β-CoGa films, obtained for an Et_3Ga mole fraction of 2.6×10^{-3}, is almost independent of the deposition temperature over the temperature range investigated (Figure 8). By contrast, for lower concentrations of Et_3Ga in the gas phase, the films have the α structure and their growth rate increased significantly with the substrate temperature with an apparent activation energy roughly estimated at 105 kJ/mol (dotted line, Figure 8).

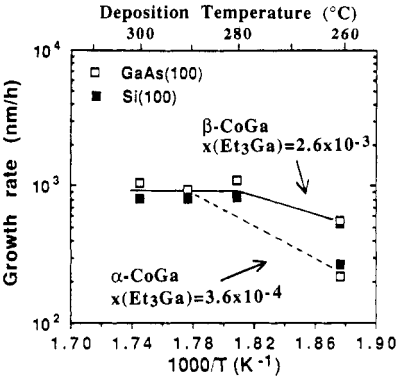

Figure 8. Variation of the growth rate of CoGa films as a function of the deposition temperature. The mole fraction of $CoCp(CO)_2$ was fixed at 2.83×10^{-4}. Data are reported for the Et_3Ga mole fractions 3.6×10^{-4} (all the samples have the α-CoGa structure) and 2.6×10^{-3} (all the samples have the β-CoGa structure) on (100)Si (■) and (100)GaAs (□).

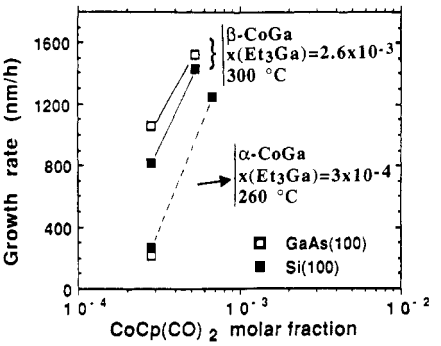

Figure 9. Variation of the growth rate of CoGa films as a function of the $CoCp(CO)_2$ mole fraction. Data are reported for the Et_3Ga mole fractions and deposition temperatures 2.6×10^{-3}/300 °C (β-CoGa structure) and 3×10^{-4}/260 °C (α-CoGa structure) on (100)Si (■) and (100)GaAs (□).

The growth rate of the films depends also on the gas-phase composition. Looking at the data for each phase, one can observe that the growth rate of the α- and β-CoGa films increases sharply with the mole fraction of $CoCp(CO)_2$ (Figure 9). On the other hand, for an increasing mole fraction of Et_3Ga by almost 2 orders of magnitude, the growth rate increases in the low concentration range but no significant variation is observed at higher concentration, either at 260 or 300 °C (Figure 10). Because there is a structural change for a mole fraction $x(Et_3Ga) > 4 \times 10^{-4}$, we emphasize from these data only that the growth rate of β-CoGa is almost independent of the Et_3Ga mole fraction. These two observations indicate that for high concentrations of the gallium source ($Et_3Ga/CoCp(CO)_2 > 9$) the process is mass transport limited presumably due to the gas-phase diffusion of the minor species $CoCp(CO)_2$.

Discussion

Epitaxial layers of CoGa have been successfully grown for the first time on (100)GaAs by OMCVD using $(\eta^5\text{-}C_5H_5)Co(CO)_2$ and $(C_2H_5)_3Ga$ as the sources of Co and Ga, respectively. The composition of these intermetallic films can be controlled from the composition of the gas phase in such a way that Ga-rich CoGa films are perfectly lattice matched to the GaAs substrate. The lattice mismatch of films containing, for instance, 55 and 64 at.

(42) Schubert, K.; Lukas, H. L.; Meissner, H.-G.; Bhan, S. *Z. Metallkde.* **1959**, *50*, 534.

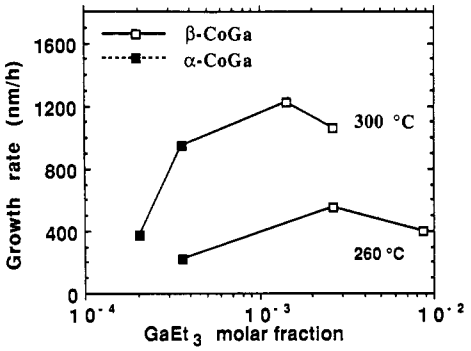

Figure 10. Variation of the growth rate of CoGa films as a function of the Et_3Ga mole fraction. All the deposition parameters were kept constant including the mole fraction of $CoCp(CO)_2$, which was fixed at 2.83×10^{-4}. Data are reported for the deposition temperatures 260 and 300 °C on (100)GaAs. They are fully supported by data on (100)Si which are not reported for clarity. The films have the α (■) and the β (□) structure.

% Ga is ~2 and ~0%. By contrast, Co-rich films exhibit the α structure of the solid solution $Co_{1-x}Ga_x$ which is considered metastable when the Ga content reaches 37 at. %.[30,40] In the following section, the consistency of these results is discussed by correlation with the preliminary kinetics data.

It is well-known in CVD processes that three distinct temperature-dependent regions of growth are identified: a low-temperature kinetically controlled growth regime, a mid-temperature mass transport limited region, and a high-temperature range where the growth rate falls off with increasing temperature (as, for example, observed for OMCVD of GaAs using either $(CH_3)_3Ga$ or Et_3Ga with AsH_3).[43] The low-temperature kinetically controlled growth regime is characterized by an apparent activation energy (usually in the range 63–210 kJ/mol) that suggests that chemisorption and heterogeneous reactions are essential to the growth. As a consequence, the deposition rate depends on the substrate orientation and such conditions generally do not lead to films of high crystallinity. In the mid-temperature regime, the growth rate is almost independent of the temperature because the surface reactions proceed faster than the diffusion of the minor species through a stagnant boundary layer above the substrate. This is the best condition for an epitaxial growth of the film. At high temperature, the decrease of the growth rate is explained by an increase of either the desorption of surface species or by depletion of reagents in the gas phase due to homogeneous decomposition.

The formation of soot on the reactor wall and on the substrates during the deposition of our CoGa films for $T > 300$ °C suggests a homogeneous (gas phase) decomposition of the precursors and precludes an investigation of the kinetic behavior in this high temperature range.

For gas phase compositions $Et_3Ga/CoCp(CO)_2 \geq 5$ (obtained, for instance, for Et_3Ga mole fraction $= 2.6 \times 10^{-3}$) the CoGa films have the β structure and they grow epitaxially on (100)GaAs. Their deposition rate is weakly dependent on the reciprocal temperature (Figure 8), revealing a mass transport limited growth regime favorable to an epitaxial growth. Furthermore, both the strong dependence of the β-CoGa growth rate upon the mole fraction of $CoCp(CO)_2$ (Figure 9) and its weak dependence upon the mole fraction of Et_3Ga (for $x(Et_3Ga) > 4 \times 10^{-4}$; Figure 10) suggest that the β-CoGa growth rate is limited by the mass transfer of the Co source, which probably occurs by diffusion through the boundary layer. The temperature range investigated (260–300 °C) is thus identified as a mid-temperature region. According to CVD models, the calculated rates in this regime are close to the calculated equilibrium-limited rates.[44] This means that, even if the diffusion is neglected, the thermodynamic predictions provide meaningful information under these conditions. In our case, the formation of a small amount of $CoGa_3$ is not surprising since the film composition is close to the boundary between β-CoGa and the biphase zone β-CoGa + CoGa3.

By contrast, α-CoGa films grown with a gas phase ratio $Et_3Ga/CoCp(CO)_2 < 5$ (i.e., Et_3Ga mole fraction $= 3.6 \times 10^{-4}$, Figure 8) in the temperature range 260–290 °C seem to display a thermally activated growth rate. In a CVD process, when the growth is kinetically controlled, this is favorable to the deposition of metastable phases that are far from thermodynamic equilibrium. Under such conditions, the CoGa films deposited consist of the α-structure supersaturated with Ga. Such a phase is structurally incompatible with GaAs and reacts above 400 °C to form CoAs (Figure 6).

These different phases probably have a different reactivity, for instance, toward the dissociative chemisorption of the CO groups. Indeed, the oxygen contamination most likely arises from a heterogeneous decomposition of the carbonyl groups in $CoCp(CO)_2$; the O and the C contaminations of the β-CoGa films was found to be lower than those in the α phase. The fact that no C or only a small amount of C is detected in these films either by XPS or Auger spectroscopy may be due to the ability of the Co constituent to convert surface carbon into volatile hydrocarbons in the presence of H_2.[45] However, the higher O contamination of the α-$Co_{1-x}Ga_x$ solid solution can be explained by a surface reactivity related to that of Co metal, which is known to dissociate the CO groups and to lead to oxide formation. In the β-CoGa compound, this particular reactivity is apparently reduced.

By contrast, with α-$Co_{1-x}Ga_x$ films which react with GaAs above 400 °C, the Ga-rich β-CoGa films are thermodynamically stable on GaAs at 500 °C as established by preliminary annealing experiments. This result is noteworthy because this is the temperature used for the epitaxial growth of GaAs by OMVPE in similar apparatus. This then suggests that the fabrication of buried metal/GaAs heterostructures will be possible by this deposition technique, parallel to recent demonstration by MBE,[2-4] when the growth of monocrystalline β-CoGa layers will be perfectly controlled.

Acknowledgment. The authors thank R. Lysse for assistance in EDX analyses. Dr. F. Maury was supported by a grant from CNRS (Centre National de la Recherche Scientifique) in cooperation with NSF (National Science Foundation). A.A.T. and R.S.W. were supported in part from a grant from SDIO administered by ONR.

(43) Reep, D. H.; Ghandhi, S. K. *J. Electrochem. Soc.* **1983**, *130*, 675.

(44) Besmann, T. M.; Spear, K. E. *J. Electrochem. Soc.* **1977**, *124*, 790.

(45) Zinn, A.; Niemer, B.; Kaesz, H. D. *Adv. Mater.* **1992**, *4*, 375.